Monthly Notices of the ROYAL ASTRONOMICAL SOCIETY

Mon. Not. R. Astron. Soc. **417,** 709–716 (2011) doi:10.1111/j.1365-2966.2011.19316.x

Qatar-1b: a hot Jupiter orbiting a metal-rich K dwarf star

K. A. Alsubai,[1★] N. R. Parley,[2] D. M. Bramich,[3] R. G. West,[4] P. M. Sorensen,[5] A. Collier Cameron,[2] D. W. Latham,[6] K. Horne,[2] D. R. Anderson,[7] G. Á. Bakos,[6] D. J. A. Brown,[2] L. A. Buchhave,[8] G. A. Esquerdo,[6] M. E. Everett,[9] G. Fűrész,[6] J. D. Hartman,[6] C. Hellier,[7] G. M. Miller,[2] D. Pollacco,[10] S. N. Quinn,[6] J. C. Smith,[11] R. P. Stefanik[6] and A. Szentgyorgyi[6]

[1]*Qatar Foundation, PO BOX 5825 Doha, Qatar*
[2]*SUPA, School of Physics and Astronomy, University of St Andrews, North Haugh, St Andrews, Fife KY16 9SS*
[3]*European Southern Observatory, Karl-Schwarzschild-Straβe 2, 85748 Garching bei München, Germany*
[4]*Department of Physics and Astronomy, University of Leicester, Leicester LE1 7RH*
[5]*Nordic Optical Telescope, Apartado 474, E-38700 Santa Cruz de la Palma, Santa Cruz de Tenerife, Spain*
[6]*Harvard–Smithsonian Center for Astrophysics, 60 Garden Street, Cambridge, MA 02138, USA*
[7]*Astrophysics Group, Keele University, Staffordshire ST5 5BG*
[8]*Niels Bohr Institute, Copenhagen University, DK-2100 Copenhagen, Denmark*
[9]*Planetary Science Institute, 1700 East Fort Lowell Road, Suite 106, Tucson, AZ 85719, USA*
[10]*Astrophysics Research Centre, School of Mathematics & Physics, Queens University, University Road, Belfast BT7 1NN*
[11]*Hidden Loft Observatory, Tucson, AZ 85755, USA*

Accepted 2011 June 23. Received 2011 May 26; in original form 2010 December 14

ABSTRACT

We report the discovery and initial characterization of Qatar-1b, a hot Jupiter-orbiting metal-rich K dwarf star, the first planet discovered by the Qatar Exoplanet Survey. We describe the strategy used to select candidate transiting planets from photometry generated by the Qatar Exoplanet Survey camera array. We examine the rate of astrophysical and other false positives found during the spectroscopic reconnaissance of the initial batch of candidates. A simultaneous fit to the follow-up radial velocities and photometry of Qatar-1b yields a planetary mass of $1.09 \pm 0.08\,M_{\rm J}$ and a radius of $1.16 \pm 0.05\,R_{\rm J}$. The orbital period and separation are $1.420\,033 \pm 0.000\,016$ d and $0.023\,43 \pm 0.000\,26$ au for an orbit assumed to be circular. The stellar density, effective temperature and rotation rate indicate an age greater than 4 Gyr for the system.

Key words: techniques: photometric – techniques: radial velocities – techniques: spectroscopic – stars: individual: Qatar-1 – planetary systems.

1 INTRODUCTION

Transiting extrasolar planets are important because measurements of the planetary transits as well as the stellar reflex velocity provide both the mass and radius, and hence the density of the planet. In contrast to the relatively tight mass–radius relationship of main-sequence stars, the hot Jupiters found in transit surveys exhibit a wide range of radii at each mass; thus additional parameters affect the radii of close-in gas giants. With over 100 transiting extrasolar planets now securely characterized (Schneider et al. 2011), statistics are beginning to support comparative studies to unravel the factors that determine their radii and orbit parameters (Mordasini et al. 2009). Towards this goal, it is important to extend the statistics of hot Jupiters to smaller planets.

In their 2001 February data release, the *Kepler* mission team announced 1235 Kepler Objects of Interest that had survived preliminary vetting (Borucki et al. 2011), providing good statistics on the orbital periods and radii of transiting bodies. Independent estimates by Morton & Johnson (2011) suggest that as many as 90 per cent of these candidates could be bona fide transiting planets. At typical distances 300–1000 pc, follow-up spectroscopic studies for high-precision radial velocities (RVs) to measure the stellar wobble and hence the masses of the smaller transiting bodies present a considerable challenge for present-generation instruments. In contrast to *Kepler*, the ground-based wide-angle exoplanet transit surveys have a bright limit imposed by CCD saturation at $V \simeq 9.0$. They attain photometric precision better than 0.01 mag (sufficient for detection of transits by gas-giant planets) in stars brighter than $V \simeq 12.5$.

★E-mail: kalsubai@qf.org.qa

The distribution of spectral types among main-sequence stars in this magnitude range peaks sharply among the late F and early G stars. There are few early-type main-sequence stars fainter than $V = 9.0$ at moderate to high Galactic latitudes. Saturn-sized to Neptune-sized planets are more easily detected if they orbit smaller stars, but dwarfs of spectral type K or later are poorly represented because the sampling volume decreases towards lower masses faster than their space density increases.

The Qatar Exoplanet Survey[1] (QES; Alsubai et al. 2011) has initiated a wide-field transit search programme deploying initially a five-camera CCD imaging system designed to go 0.5 mag deeper than most current wide-angle survey systems such as Super Wide-Area Search for Planets (SuperWASP),[2] Hungarian Automated Telescope Network (HATNet),[3] Tillinghast Reflector Echelle Spectrograph (TRES)[4] and XO.[5] The QES's first site in New Mexico was chosen to complement the SuperWASP sites in the Canary Islands and South Africa, where suites of eight 200-mm f/1.8 Canon lenses image $16° \times 32°$ fields at 15 arcsec pixel^{-1}. The QES camera system images an $11° \times 11°$ field of view simultaneously at two pixel scales. A single 200-mm f/2.0 Canon lens covers the full $11° \times 11°$ field at 9.26 arcsec pixel^{-1}. Four 400-mm f/2.8 Canon lenses each cover $5.5° \times 5.5°$ fields arranged in a 2×2 mosaic to cover the same $11° \times 11°$ field. The QES cameras' higher angular resolution and larger aperture yield a magnitude limit 0.5 mag fainter than those of WASP or HAT. This doubles the sampling volume for low-mass stars, extending the search for transiting planets to stars with smaller radii that are none the less bright enough for RV follow-up with 2 to 4 m class telescopes. Combining QES and SuperWASP data should increase the exoplanet discovery rate by enabling multiple transits of candidate systems to be obtained more quickly.

This paper reports the discovery and initial characterization of the first confirmed transiting exoplanet to emerge from the QES, orbiting the star 3UC311−087990 (Qatar-1, $\alpha_{2000} = 20^{\rm h}\ 13^{\rm m}\ 31\overset{\rm s}{.}61$, $\delta_{2000} = +65°\ 09'\ 43\overset{''}{.}4$). The survey observations and candidate selection procedures that led to the discovery of Qatar-1b are presented in Section 2, together with our analysis of the stellar spectrum and follow-up photometry. We discuss in Section 3 our determination of the stellar and planetary system parameters, leading to the summary and conclusions in Section 4.

2 OBSERVATIONS

The QES cameras use FL1 ProLine PL6801 KAF-1680E 4k×4k CCD detectors. The robotic mount cycles through four pointings, taking 100-s exposures with the 400-mm cameras and 60-s exposures with the 200-mm camera, thereby covering a $\sim$400 deg^2 field with a cadence of 8 min. The 400-mm lenses target stars between $V = 11$ and 15 mag with 100-s exposures, while the 200-mm lens covers the magnitude range from $V = 8$ to 12 mag with 60-s exposures. We thus obtain photometry of all stars in the field in the range from $V = 8$ to 15 mag.

The data are reduced at the University of St Andrews using pipeline software based on the image-subtraction algorithm of Bramich (2008). A detailed description of the pipeline is given by Alsubai et al. (2011). The pipeline data products are ingested into a data archive at the University of Leicester, which uses the same architecture as the WASP archive (Pollacco et al. 2006).

2.1 Discovery photometry

An automated transit search was conducted on the archive data using the box least-squares (BLS) algorithm of Kovács, Zucker & Mazeh (2002) as modified for the SuperWASP project by Collier Cameron et al. (2006). Systematic patterns of correlated noise were modelled and removed from the archive light curves using a combination of the SysRem algorithm of Tamuz, Mazeh & Zucker (2005) and the trend filtering algorithm (TFA) of Kovács, Bakos & Noyes (2005). The light curves of all candidates were subjected to the candidate screening tests described by Collier Cameron et al. (2007) to ensure that the depths and durations of the transits were consistent with expectation for objects of planetary dimensions transiting main-sequence stars. In cases where the same star had been observed by the SuperWASP survey, we ran periodogram tests to seek evidence of a transit signal in the SuperWASP data at the same period.

The star 3UC311−087990 was observed in two survey fields of the QES instrument. Field 195525+634100 was observed 1594 times from 2010 Jun 16 to September 24, whilst field 200400+653000 was observed 1379 times during the same time interval. The star was found to exhibit transit-like events at 1.42-d intervals in the individual field 200400+653000 and in searches of the combined data from the two fields. These fields are to the north of the declination limit of the SuperWASP survey, so no SuperWASP light curve was available. The star 3UC311−087990 exhibited a clear transit signal with signal detection efficiencies (as defined by Kovács et al. 2002) SDE = 10 and 22, respectively, for the individual field and the combined data. The corresponding signal-to-red noise ratios were $S_{\rm red} = 10.3$ and 12.6 using the definition of Collier Cameron et al. (2006).

The transit duration and $J - H$ colour of 3UC311−087990 were found to be consistent with the radius and mass of a main-sequence K dwarf host. For such a star, the 0.02-mag transit depth (Fig. 1) suggests a companion radius close to that of Jupiter.

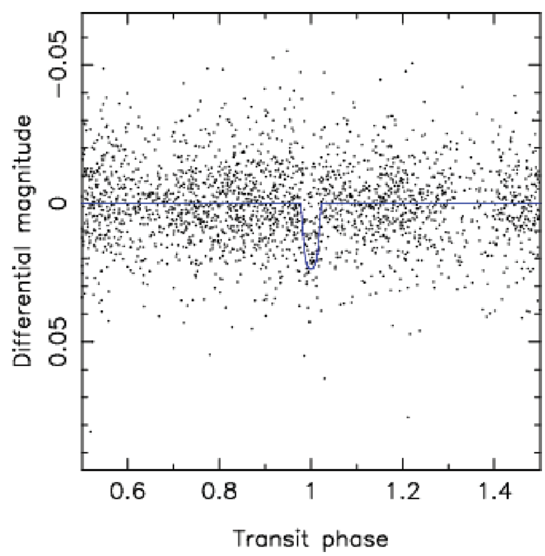

Figure 1. QES discovery light curve of Qatar-1b. The data are phase folded using the ephemeris HJD = 245 5518.4102 + 1.420 033*E*. The solid line represents the best-fitting model transit light curve derived from these observations and the follow-up RVs and photometry.

[1] http://www.alsubaiproject.org/default.aspx
[2] see http://www.superwasp.org/
[3] http://www.hatnet.hu/
[4] http://dl.dropbox.com/u/502281/Sites/solas/tres/tres.html
[5] http://www-int.stsci.edu/~pmcc/xo/

2.2 Spectroscopic reconnaissance

A list of 28 candidates was provided by the QES to the Harvard–Smithsonian Center for Astrophysics (CfA) team in 2010 November. The usual first step at the CfA for vetting transiting-planet candidates from wide-angle ground-based photometric surveys is to obtain reconnaissance spectra with the TRES on the 1.5-m Tillinghast Reflector at the Fred L. Whipple Observatory operated by the Smithsonian Astrophysical Observatory (SAO) on Mount Hopkins in Southern Arizona. These spectra are used to look for evidence of stellar systems that are the source of the transit-like light curves (e.g. see Latham et al. 2009) and also to provide refined stellar parameters for the targets.

An initial spectroscopic reconnaissance was carried out for all 28 candidates, based on 60 spectroscopic observations with TRES over a span of 17 nights. We used the medium fibre (2.3-arcsec projected diameter), yielding a resolving power of $R \simeq 48\,000$, giving a wavelength coverage of ~3800–9100 Å. We used the wavelength range from approximately ~4400–6800 Å to determine the RVs. The exposure time was approximately 50 min, yielding a signal-to-noise ratio (S/N) from 20 to 25 per pixel in the Mg *b* region.

The spectra were rectified and cross-correlated using a custom-built pipeline designed to provide precise RVs for échelle spectrographs. The procedures are described in more detail in Buchhave et al. (2010). Each science exposure is bracketed by two thorium–argon (ThAr) calibration images which are combined to form the basis for the fiducial wavelength calibration. Once the spectra have been extracted, a cross-correlation is performed order by order. The orders are cross-correlated using a fast Fourier transform (FFT) and the cross-correlation functions (CCFs) for all the orders co-added and fitted with a Gaussian function to determine the RV. Uncertainties of the individual velocities were estimated by $\sigma = \mathrm{rms}(v)/\sqrt{N}$, where v is the RV of the individual orders and N is the number of orders. A summary of the candidates and the results of the reconnaissance are reported in Table 1.

For the initial analysis, the TRES spectra are correlated against a library of synthetic spectra. This provides useful information about the characteristics of the target star, such as effective temperature, surface gravity and rotational and absolute RV, but it only uses a small fraction of the full 390–900 nm spectral range of TRES. To look for evidence of low-amplitude orbital motion, we take advantage of the wide wavelength coverage by correlating the individual observations of a star against a template derived from observations of the same star, either a single observation that has especially strong S/N or a master observed template constructed by shifting and co-adding all the observations of the star.

The RVs reported in Table 1 are calibrated using an absolute velocity zero-point based on observations of the International Astronomical Union (IAU) RV standard star HD 182488. The *Kepler* team has agreed to use this as the standard for the reconnaissance spectroscopy of Kepler Objects of Interest. We have adopted the velocity of $-21.508\ \mathrm{km\,s^{-1}}$ as the value on the IAU system for HD 182488. During the November run, we accumulated 15 strong observations of HD 182488, giving an observed mean velocity on the TRES native system of $-20.807 \pm 0.057\ \mathrm{km\,s^{-1}}$, where the error is the rms residuals from the mean. This is an offset of $+0.701\ \mathrm{km\,s^{-1}}$ from the adopted IAU velocity for HD 182488. The RVs reported in Table 1 have had this offset applied, to bring them as closely as possible into line with the RV of HD 182488 on the IAU system.

When many candidates are being vetted, it is efficient to schedule the initial observations near times of quadrature, as predicted from the photometric ephemerides. In the case of double-lined binaries that are undergoing grazing eclipses, this guarantees that the velocities of the two stars will be near their maximum separation, and thus a single spectrum will be sufficient for rejecting the target if it shows a composite spectrum. If the first observation reveals the spectrum of just one star, a second observation near the opposite quadrature is optimum for disclosing orbital motion due to unseen stellar companions. Of course, this assumes that the photometric ephemeris has the correct period and is up to date.

The false positive rate is a strong function of the strategy of the project and the threshold for selecting candidates, which was deliberately set low for this preliminary follow-up campaign. 11 stars among the original candidate list showed weak but plausible candidate signals in only one QES camera, but showed no corresponding signal in their WASP light curves. We included them in order to investigate the extent to which corroborating evidence from WASP or another QES camera was necessary to guarantee the reality of a faint candidate signal. Seven among these candidates showed no significant velocity variations. Careful inspection of the available light curves and BLS periodograms supported the interpretation that the transit detections were false alarms, with SDE <8 and/or $S_{\mathrm{red}} < 8$. By contrast, there were no false alarms among targets where the QES signal was found to be also present in WASP data, or where the same signal was seen in two QES cameras. We conclude from this that weak candidates for which independent data exist but no corresponding signal is found have a far lower yield than candidates of comparable signal strength with two or more independent signal detections. The very low rate of RV non-detections among targets with independently confirmed periods illustrates the advantage of the improved plate scale and image size of QES data (relative to WASP) in reducing contamination by faint eclipsing binaries at small angular separations.

Nine of the candidates showed clear evidence of stellar companions in their spectra. In eight cases, the initial reconnaissance observation revealed a composite spectrum with at least two sets of lines, with evidence that three stars were likely to be involved for two of the targets. For the ninth case, the spectrum was single lined, but with a very large change in velocity between the two observations. Three of the candidates showed broad lines corresponding to equatorial rotational velocities of tens of $\mathrm{km\,s^{-1}}$, which would render impractical the measurement of very precise RVs, and two of the candidates proved to have temperatures corresponding to late A stars. In three cases, the classification of the TRES spectra indicated that the targets are giants, presumably bright stars diluting the light of eclipsing binaries, either in hierarchical triple systems or accidental alignments.

Two of the candidates with secure transit detections showed very small velocity variations that could be consistent with orbital motion due to planetary companions, and one candidate that was observed only once showed a spectrum suitable for very precise velocity measurements. These three targets deserve additional follow-up. Finally, one of the candidates (3UC311−087990, hereinafter referred to as Qatar-1) was confirmed as a system with a transiting planet, as described in the following sections.

2.3 Radial velocity follow-up

The first two RVs of Qatar-1, obtained near opposite quadratures, showed a small but significant difference consistent with the photometric ephemeris and with the interpretation of a planetary mass for the companion. Subsequently, this star was observed every clear night with a longer exposure time of 54 min, with the goal of deriving an orbital solution. The multi-order relative RVs from all

Table 1. QES transiting planet candidates.

Candidate	α_{2000}	δ_{2000}	V (mag)	Period (d)	Epoch (HJD)	SDE	$S_{\rm red}$	$T_{\rm eff}$ (K)	log (g)	$V_{\rm rot}$ (km s^{-1})	$V_{\rm rad}$ (km s^{-1})	σ_V (km s^{-1})	$N_{\rm obs}$	Exp. time (min)	Field	Type
215−018836	04:20:29.30	17:03:29.0	11.7	2.6539	245 5182.031 87	6.5	6.7	5000	3.00	6	32.050	–	1	30	Q1	G
210−017759	04:23:18.22	14:58:19.2	14.2	1.6343	245 5170.024 98	7.6	7.4	7750	5.00	6	0.737	0.860	2	105	Q1W0	H
214−019086	04:25:10.26	16:49:59.9	14.8	2.1799	245 5186.897 30	6.6	6.8	6250	4.50	60	−5.823	–	1	80	Q1W1	FR
214−019418	04:27:58.86	16:55:21.8	13.3	1.2068	245 5510.834 00	5.8	5.7	6125	3.75	7	−41.841	0.075	2	70	Q1W0	FA?
214−019710	04:30:22.44	16:54:27.1	14.0	2.3042	245 5180.037 81	12.0	8.3	6250	5.00	25	−5.879	–	1	45	Q1W0	–
216−021225	04:35:04.30	17:35:27.9	13.3	1.2131	245 5154.588 90	8.2	7.1	5875	3.75	7	13.823	0.078	2	54	Q1W0	FA?
212−019540	04:35:15.20	15:30:57.9	12.6	5.2482	245 5155.242 80	7.1	7.4	6125	3.50	45	−1.858	1.281	2	80	Q1	FR
197−017651	04:38:58.36	08:13:15.0	13.3	1.3681	245 5511.602 00	10.2	5.9	6750	4.00	9	86.048	0.061	3	76	Q1W0	FA?
183−015913	04:41:57.49	01:24:48.7	12.5	1.5418	245 5178.869 96	10.0	12.8	6250	3.50	20	64.420	–	1	24	Q1	D
210−019969	04:45:41.07	14:43:21.6	13.1	1.9023	245 5154.866 90	9.7	9.5	5250	4.50	25	26.303	–	1	24	Q1W0	D
217−022884	04:47:31.64	18:29:08.8	13.1	2.1060	245 5155.621 50	6.1	6.5	6875	4.00	28	−6.508	0.434	2	47	Q1W0	H
184−018774	05:03:22.93	01:45:07.2	13.4	1.8672	245 5154.955 50	13.6	10.2	6750	3.50	20	−22.110	–	1	30	Q2W1	D
194−020871	05:03:59.84	06:48:36.8	13.2	2.3520	245 5184.593 28	15.8	7.8	6000	5.00	16	−19.136	–	1	30	Q1W1	D
197−023150	05:09:14.35	08:16:52.8	12.2	4.2357	245 5156.639 30	7.4	11.0	6000	4.00	8	−8.243	0.169	2	60	Q1W0	FA?
199−022618	05:09:35.29	09:17:43.2	14.1	1.7068	245 5182.416 70	10.4	9.7	6500	4.00	30	40.073	54.218	2	84	Q1W1	S
196−023727	05:16:02.99	07:37:03.4	13.7	1.8731	245 5154.930 60	7.2	9.2	4750	4.50	1	−11.494	0.118	3	150	Q1W0	FA?
205−023986	05:25:06.47	12:04:33.7	11.3	5.2372	245 5175.610 72	7.6	6.9	5000	3.00	4	27.900	–	1	15	Q1	G
190−024393	05:28:13.25	04:42:24.4	13.3	1.3150	245 5180.882 87	8.2	8.2	5417	4.33	3	29.785	0.267	6	289	Q1W0	FA?
210−028815	05:30:41.80	14:54:49.0	12.9	2.8459	245 5155.231 50	8.5	8.1	6000	3.75	9	28.885	0.121	2	87	Q1	P?
308−105347	18:51:21.19	63:59:02.5	12.8	1.5758	245 5365.009 60	19.9	9.9	6500	3.50	45	−113.203	–	1	30	Q2W1	D
284−137549	18:59:30.39	51:34:50.0	12.4	2.4046	245 5365.534 30	17.4	9.6	6000	3.00	45	19.963	–	1	24	Q1W1	T?
304−111233	19:22:52.65	61:53:48.6	13.3	2.0262	245 5510.610 00	–	–	5250	4.50	110	−14.707	–	1	30	Q2W0	FR
309−100007	19:25:15.34	64:00:17.9	13.2	2.1804	245 5407.446 53	–	–	5625	4.38	3	−36.859	0.161	4	175	Q1W0	FA?
301−128216	19:32:07.33	60:27:07.0	13.7	1.8227	245 5364.683 00	7.2	4.2	5250	4.00	2	1.529	0.104	2	74	Q2W0	P?
301−128743	19:35:42.56	60:27:05.4	12.5	1.0851	245 5413.400 90	23.2	8.2	6083	4.00	6	−28.514	13.803	3	72	Q2W1	T?
294−143877	19:45:11.25	56:35:16.3	12.2	1.3284	245 5424.537 73	19.4	15.0	6250	4.50	4	−95.671	–	1	30	Q2W1	D
311−087990	20:13:31.61	65:09:43.4	12.6	1.4201	245 5407.649 00	22.1	12.3	4861	4.44	2	−37.900	0.189	9	472	Q2	P!
294−152358	20:20:22.74	56:32:25.0	13.0	2.3267	245 5365.327 40	6.7	6.4	5000	3.50	3	−72.159	0.126	2	60	Q1W0	G?

Note. The columns are labelled as follows. Column 1: UCAC3 identification for the target; columns 2 and 3: J2000 right ascension and declination measured by this project; column 4: V magnitude from QES pipeline calibration against UCAC3 magnitude; columns 5–8: photometric period and epoch, BLS signal detection efficiency and signal-to-red noise ratio; columns 9–11: effective temperature, log surface gravity and rotational line broadening of the synthetic template spectrum that gave the best match to the observed spectra, assuming solar metallicity; columns 12 and 13: absolute RV on the IAU system and rms variation when two or more measurements were obtained; columns 14 and 15: number of TRES observations and total exposure time; column 16: detection summary – Qn means the transits were detected by n of the QES cameras, W1 means the transits were also detected with the same period by SuperWASP, W0 means that SuperWASP did not confirm the detection and no W means the target field was not observed by SuperWASP; column 17: disposition of the candidate – D = the spectrum shows two sets of lines, FA? = a likely photometric false alarm, FR = a rapidly rotating star for which precise RVs are not feasible, G = a giant, presumably in a blended system with an eclipsing binary, G? = a likely giant, H = a hot star, P? = the velocity variations are small and not inconsistent with a planetary companion, P! = a confirmed planetary companion, S = the spectrum is single-lined and shows a large velocity variation due to a stellar companion, T? = a likely triple system.

Table 2. Relative RVs for Qatar-1.

BJD (d)	Phase	Radial velocity ($\mathrm{km\,s^{-1}}$)	Bisector span ($\mathrm{km\,s^{-1}}$)
245 5518.696 28	0.2014	-0.1297 ± 0.0605	0.0068 ± 0.0443
245 5519.591 74	0.8320	0.3515 ± 0.0292	-0.0227 ± 0.0131
245 5520.632 31	0.5648	0.2411 ± 0.0462	0.0164 ± 0.0296
245 5521.584 09	0.2350	-0.0663 ± 0.0407	0.0127 ± 0.0166
245 5523.609 08	0.6610	0.2611 ± 0.0261	-0.0045 ± 0.0143
245 5525.592 98	0.0581	0.0 ± 0.0221	-0.0065 ± 0.0088
245 5526.587 11	0.7582	0.3618 ± 0.0458	0.0037 ± 0.0219
245 5527.591 21	0.4653	0.0854 ± 0.0221	-0.0179 ± 0.0128
245 5528.584 27	0.1646	-0.0403 ± 0.0305	0.0120 ± 0.0117

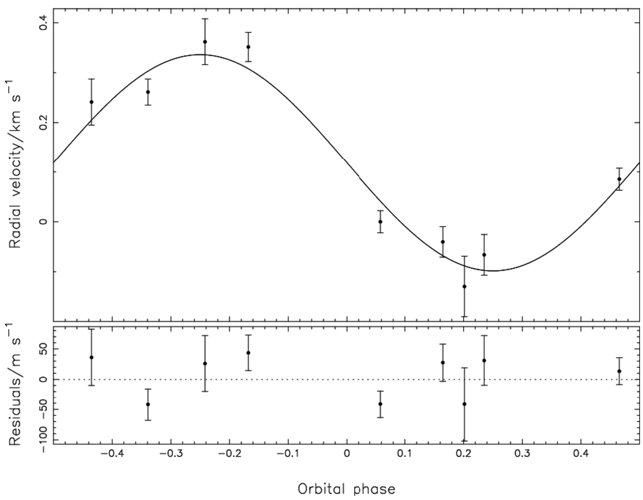

Figure 2. Upper panel: relative RV data for Qatar-1, with 1σ error bars, phase folded on the ephemeris given in Table 3. The best-fitting circular orbit model (solid line) is also shown. Lower panel: residuals of the fit to the best-fitting circular orbit model.

nine observations of Qatar-1 are reported in Table 2 and are plotted in Fig. 2 together with a circular orbit, phased to the period and epoch of the photometric ephemeris. No significant correlation was found between the variation in the line bisectors and the relative RVs, as shown in Fig. 3. Thus there is no evidence in the TRES spectra that the RV variations are due to phenomena other than orbital motion, such as an unresolved blend with a faint eclipsing binary or spots coupled with stellar rotation (Queloz et al. 2001).

2.4 Spectroscopic parameters of Qatar-1

As mentioned in Section 1, a transiting planet allows us to determine both the radius and the mass of the planet, if a spectroscopic orbit for the host star is available to complement the transit light curve. This in turn provides key information about the bulk properties of the planet, such as density. However, the planetary mass and radius values are relative to the mass and radius of the host star, and the accuracy with which the planetary properties can be determined is often limited by the uncertainties in the characteristics of the host star. Nearby stars with accurate parallaxes have the advantage that the observed luminosity of the star helps pin down key stellar parameters such as radius and effective temperature. For more distant stars, such as Qatar-1, the alternative is to use stellar models together with values for the effective temperature and metallicity derived from the spectra.

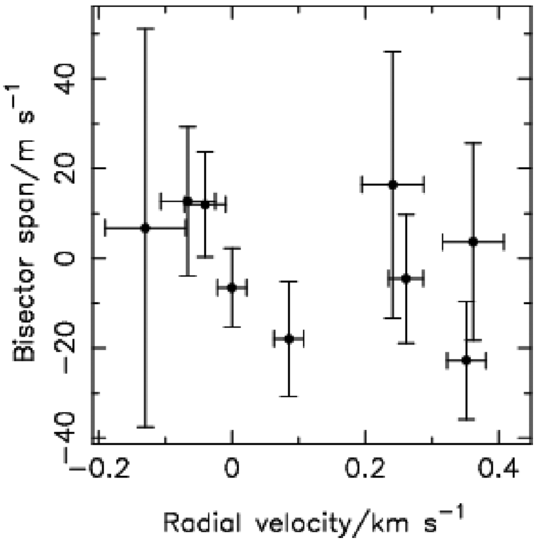

Figure 3. Line bisector span versus RV for Qatar-1.

We have used our library of synthetic spectra and a correlation analysis of our TRES spectra similar to that described by Torres, Neuhäuser & Guenther (2002) to derive the following results for Qatar-1: effective temperature $T_{\mathrm{eff}\star} = 4861 \pm 125$ K, surface gravity $\log g_\star = 4.40 \pm 0.1$ (log cgs), projected rotational velocity[6] $v \sin I = 2.1 \pm 0.8\,\mathrm{km\,s^{-1}}$ and metallicity [Fe/H] $= +0.20 \pm 0.1$ dex. The observed spectra are cross-correlated against a grid of synthetic spectra drawn from a library calculated by John Laird using Kurucz models (Kurucz 1992) and a line list prepared by Jon Morse. The synthetic spectra cover a window of 300 Å centred near the gravity-sensitive Mg *b* features and has a spacing of 250 K in effective temperature, 0.5 dex in gravity, 0.5 dex in metallicity and 1 $\mathrm{km\,s^{-1}}$ in rotational velocity. The best matched template to the observed spectrum represents the best matched stellar parameters on the library grid. A new set of tools is then used to derive more precise stellar parameters from the normalized cross-correlation peaks. A description of the tools will be published by Buchhave et al. (in preparation). Spectroscopic determinations of stellar surface gravity are notoriously difficult, so it is fortunate that $\log g_\star$ can be determined independently from a joint analysis of the transit light curve and spectroscopic orbit. For Qatar-1 that analysis yielded $\log g_\star = 4.53 \pm 0.02$, as described in the next section.

The stellar parameters adopted for the host star are listed in Table 3 together with catalogue magnitudes and additional stellar dimensions obtained by fitting a model to the transit profiles and spectroscopic orbit.

2.5 Follow-up photometry

A full transit of the planet Qatar-1b was observable from high northern latitudes on the night of 2010 November 27. *R*-band photometry was obtained of the ingress with the CCD camera on the 0.95-m James Gregory Telescope (JGT) located at St Andrews, Scotland, during the transit of 2010 November 27. A total of 25 180-s exposures was obtained in clear conditions, but the sequence was terminated early by snow clouds. The egress of the same November

[6] The symbol I represents the inclination of the stellar rotation axis to the line of sight, whereas i is used elsewhere in this paper to denote the orbital inclination.

Table 3. Stellar parameters for Qatar-1 derived from spectroscopic reconnaissance, photometric catalogues and model fitting.

Spectroscopic parameter	Value	Source
$T_{\mathrm{eff}\star}$ (K)	4861 ± 125 K	TRES
[Fe/H]	0.20 ± 0.10	TRES
$v \sin I$ (km s^{-1})	2.1 ± 0.8	TRES
γ_{RV} (km s^{-1})	-37.835 ± 0.063	TRES
Photometric parameter	Value	Source
V (mag)	12.843 ± 0.137	TASS4
J (mag)	10.999 ± 0.021	2MASS
H (mag)	10.527 ± 0.019	2MASS
K_{s} (mag)	10.409 ± 0.017	2MASS
Model parameter	Value	Source
$M_\star$ ($\mathrm{M}_\odot$)	0.85 ± 0.03	MCMC
$R_\star$ ($\mathrm{R}_\odot$)	0.823 ± 0.025	MCMC
$\rho_\star$ ($\rho_\odot$)	1.52 ± 0.12	MCMC
$\log g$ (cgs)	4.536 ± 0.024	MCMC
Age (Gyr)	>4	MCMC+YY

27 transit was observed in clear conditions with the 60-cm telescope and CCD camera of the University of Keele. A sequence of 535 20-s R-band measurements was obtained. Stellar fluxes were extracted from the CCD images following bias subtraction and flat-fielding, using the aperture photometry routines of the PHOTOM package distributed as part of the Starlink Software Collection.[7] Differential photometry was performed relative to nearby stars on the same CCD images.

Using the refined ephemeris from these observations, we identified an opportunity to observe a complete transit using the KeplerCam CCD on the Fred Lawrence Whipple Observatory (FLWO) 1.2-m telescope on the evening of 2010 December 2. The transit was observed using 90-s exposures in the Sloan i filter; the reduction of these images to light curves, including basic calibration, astrometry, aperture photometry, ensemble magnitude calibration and decorrelation against external parameters, was performed following the method described by Bakos et al. (2010). For the external parameter decorrelation, we fitted for the trends using only the out-of-transit data and applied the resulting correction to the full light curve.

A third transit was observed in its entirety on 2010 December 7, again using the JGT with an R-band filter.

The four follow-up light curves are shown, together with the best-fitting model, in Fig. 4. The transit is seen to be slightly more than 0.02 mag deep in both wavelength bands. The i-band light curve in particular shows four well-defined contacts but rather lengthy ingress and egress phases, suggesting a moderately high impact parameter.

3 STELLAR AND PLANETARY DIMENSIONS

The dimensions of the planet and its host star were determined from a simultaneous model fitted to the RVs and the combined photometry from the QES cameras and follow-up transit observations. The transit light curve was modelled using the formulation of Mandel & Agol (2002) in the small-planet approximation. A four-coefficient non-linear limb-darkening model was used, employing fixed co-

[7] http://starlink.jach.hawaii.edu/starlink

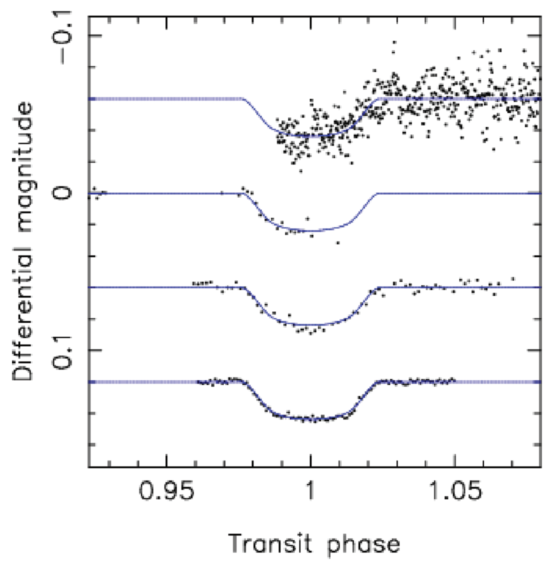

Figure 4. Photometric follow-up light curves, offset from each other by an arbitrary amount for clarity. From top to bottom: R-band photometry of the planetary egress obtained using the Keele 60-cm telescope, 2010 November 27; R-band photometry of the November 27 planetary ingress obtained using the 0.95-m JGT; R-band JGT photometry of the December 7 transit; Sloan i-band photometry of the December 2 planetary transit obtained using KeplerCam on the 1.2-m telescope at FLWO. All data have been phase folded on the ephemeris given in Table 3. The best-fitting model transit light curve is overplotted in all three cases.

efficients appropriate to the R band for the QES, JGT and Keele photometry, and to the Sloan i band for the KeplerCam photometry. These were interpolated to the appropriate effective temperature and metallicity from the tabulation of Claret (2004).

The parameter optimization was performed using the current version of the Markov chain Monte Carlo (MCMC) code described by Collier Cameron et al. (2007) and Pollacco et al. (2008). The transit light curve is modelled in terms of the epoch T_0 of mid-transit, the orbital period P, the ratio of radii $d = (R_{\mathrm{p}}/R_\star)^2$, the approximate duration t_{T} of the transit from initial to final contact and the impact parameter $b = a \cos i / R_\star$. The RV orbit is defined by the stellar orbital velocity semi-amplitude $K_\star$ and the offset $\Delta\gamma$ of the centre-of-mass velocity from the zero-point of the relative velocities listed in Table 2. Where the eccentricity is allowed to float, the two additional fitting parameters $e \cos \omega$ and $e \sin \omega$ are introduced, as recommended by Ford (2006).

The linear scale of the system depends on the orbital separation a, which through Kepler's third law depends on the stellar mass $M_\star$. The stellar mass was estimated at each step in the Markov chain as a function of the effective temperature, metallicity and density of the star (Enoch et al. 2010). The effective temperature and metallicity were treated as additional MCMC model parameters, constrained by Gaussian priors with mean values and variances derived directly from the stellar spectra, as listed in Table 3.

A model fit for an eccentric orbit yields an orbital eccentricity $e = 0.23 \pm 0.11$. The uncertainty in the eccentricity and the orientation of the orbit yields a more highly inflated and uncertain value for the stellar radius, $R_\star = 1.04 \pm 0.11\,\mathrm{R}_\odot$. The planet's radius and density are similarly affected. The stellar mass increases to $0.87 \pm 0.03\,\mathrm{M}_\odot$. A star of this mass would have to be among the oldest in the Galactic disc population to have evolved to such a large radius. A more likely explanation is that the best-fitting value of the eccentricity is spurious and that the orbit is close to circular.

Table 4. System parameters and 1σ error limits derived from the MCMC analysis. Although for reasons given in the text we adopt the circular orbit solution, we include the eccentric solution here to show its influence on other system parameters.

Parameter	Symbol	Circular	Eccentric	Units
Transit epoch	T_0	5518.4102 ± 0.0002	5518.4103 ± 0.0003	(d)
Orbital period	P	1.420033 ± 0.000016	1.420033 ± 0.000015	(d)
Planet/star area ratio	$(R_p/R_*)^2$	0.02117 ± 0.00045	0.02114 ± 0.00045	
Transit duration	t_T	0.06716 ± 0.00077	0.06632 ± 0.00095	(d)
Impact parameter	b	$0.696^{+0.021}_{-0.024}$	$0.695^{+0.020}_{-0.024}$	(R_*)
Stellar reflex velocity	K_1	$0.218^{+0.015}_{-0.016}$	$0.220^{+0.015}_{-0.016}$	(km s^{-1})
Centre-of-mass velocity offset	$\Delta\gamma$	$0.118794^{+0.000052}_{-0.000053}$	$0.1336^{+0.0081}_{-0.0080}$	(km s^{-1})
Orbital eccentricity	e	0.0 (fixed)	$0.24^{+0.10}_{-0.12}$	
Longitude of periastron	ω	–	$84.6^{+11.9}_{-10.1}$	(°)
Orbital inclination	i	$83.47^{+0.40}_{-0.36}$	$79.4^{+2.3}_{-2.9}$	(°)
Orbital semimajor axis	a	$0.02343^{+0.00026}_{-0.00025}$	$0.02363^{+0.00030}_{-0.00029}$	(au)
Planet radius	R_p	1.164 ± 0.045	1.47 ± 0.16	(R_J)
Planet mass	M_p	$1.090^{+0.084}_{-0.081}$	$1.132^{+0.096}_{-0.087}$	(M_J)
Planet surface gravity	$\log g_p$	$3.265^{+0.044}_{-0.045}$	$3.078^{+0.091}_{-0.076}$	(cgs)
Planet density	ρ_p	$0.690^{+0.098}_{-0.084}$	$0.355^{+0.139}_{-0.086}$	(ρ_J)
Planet temperature	T_{eq}	1399 ± 42	1564 ± 94	(K)

The improvement in the fit resulting from the addition of $e\cos\omega$ and $e\sin\omega$ as fitting parameters is insufficient to justify adoption of anything other than a circular orbit. The F-test approach of Lucy & Sweeney (1971) indicates that there is a 16.8 per cent probability that the improvement in the fit could have arisen by chance if the underlying orbit were circular. In the absence of conclusive evidence to the contrary, we adopted the circular orbit model.

The orbital and planetary parameters derived from the MCMC model fit are summarized in Table 4.

4 DISCUSSION AND CONCLUSIONS

The spectroscopic analysis of the host star Qatar-1 indicates that it is a slowly rotating, slightly metal-rich dwarf star of spectral type K3V. The MCMC analysis of the transit duration and impact parameter yields a direct estimate of the stellar density. When compared with evolutionary tracks and isochrones for [Fe/H] = 0.2 in the $(\rho_\star/\rho_\odot)^{1/3}$ versus T_{eff} plane (Fig. 5), the spectroscopically measured effective temperature indicates a mass between 0.76 and 0.87 M$_\odot$, in good agreement with the MCMC estimate using the calibration of Enoch et al. (2010). The stellar density derived from the MCMC analysis is substantially lower than would be expected for a star of this age on the zero-age main sequence, giving a lower limit on the stellar age of 4 Gyr. The slow stellar rotation rate derived from the spectra is also consistent with a spin-down age >4 Gyr.

The planet Qatar-1b is 10 per cent more massive than Jupiter and has a radius 16 per cent greater than Jupiter's. It orbits its primary every 34 h, making it one of the shortest period planets yet found orbiting a star less massive than the Sun. The blackbody equilibrium temperature given in Table 4 is calculated assuming a planetary albedo of zero and isotropic reradiation of the power received from the host star. A more general estimate of the dayside temperature is derived directly by from the irradiating flux via the relation $T^4_{eql} = T^4_\star(R_\star/2a)^2((1-A)/F)$, where A is the planet's Bond albedo and F is the fraction of the stellar surface that reradiates at T_{eql}. Measurements of starlight reflected at optical wavelengths from the dayside hemispheres of the hot Jupiters HD 209458b (Rowe et al. 2008) and CoRoT-2b (Alonso et al. 2009) indicate that their albedos are typically of the order of a few per cent. The blackbody value of 1399 K thus constitutes a reasonably lower limit on the planet's dayside temperature.

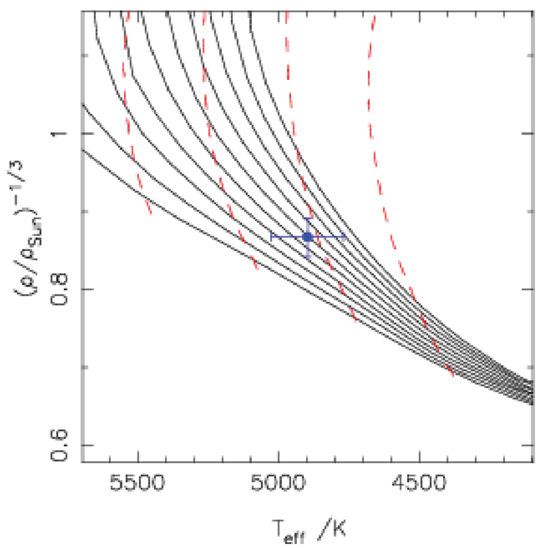

Figure 5. The position of Qatar-1 in the $(\rho_*/\rho_\odot)^{-1/3}$ plane compared to theoretical evolutionary tracks and isochrones interpolated from Yi, Kim & Demarque (2003) to [Fe/H] = 0.2. The isochrones displayed represent 2.0, 4.0, 6.0, 8.0, 10.0, 12.0, 14.0, 16.0, 18.0 and 20.0 Gyr. The evolutionary tracks represent 0.7, 0.8, 0.9 and 1.0 M$_\odot$.

Many hot Jupiters lie significantly above the mass–radius relation expected for gas-giant planets composed primarily of hydrogen and helium. As the number of transiting planets with well-determined radii has grown, a significant correlation has begun to emerge between the stellar flux irradiating the planet and the radius excess. Guillot & Showman (2002) pointed out that if even a fraction of 1 per cent of the irradiating flux were advected into the deep planetary interior, it would supply sufficient internal energy to maintain the observed inflated radii. More recently, Enoch et al. (2011) and

Laughlin, Crismani & Adams (2011) have demonstrated a strong correlation between planetary radius and irradiating flux. Among the known transiting planets, the nearest counterparts to Qatar-1b in terms of planet mass and irradiating flux are HD189733b and OGLE-TR-182b. The radii of all three planets are identical within each other's measurement errors.

Qatar-1b was one of the very first batch of transit candidates from the QES to be subjected to spectroscopic reconnaissance and RV follow-up. The rapidity of the discovery, and the fact that the planet orbits a mid-K dwarf, confirms that the instrument is well suited to the efficient discovery of planets around lower main-sequence stars.

ACKNOWLEDGMENTS

This research has made use of the ESO Data Archive, the NASA Astrophysics Data System and the VizieR catalogue access tool, CDS, Strasbourg, France. The high quality of the JGT photometry reported in this paper owes much to recent telescope upgrades made possible by a generous grant from Spanoptic Ltd of Glenrothes, and carried out with inspired technical effort by Mark Ross, Chris Booth, Roger Stapleton and David Steven. We thank the anonymous referee for several insightful suggestions for improving the clarity of the manuscript and the interpretation of the results.

REFERENCES

Alonso R., Guillot T., Mazeh T., Aigrain S., Alapini A., Barge P., Hatzes A., Pont F., 2009, A&A, 501, L23
Alsubai K. et al., 2011, PASP, submitted
Bakos G. Á. et al., 2010, ApJ, 710, 1724
Borucki W. J. et al., 2011, ApJ, 736, 19
Bramich D. M., 2008, MNRAS, 386, L77
Buchhave L. A. et al., 2010, ApJ, 720, 1118
Claret A., 2004, A&A, 428, 1001
Collier Cameron A. et al., 2006, MNRAS, 373, 799
Collier Cameron A. et al., 2007, MNRAS, 380, 1230
Enoch B., Collier Cameron A., Parley N. R., Hebb L., 2010, A&A, 516, A33
Enoch B. et al., 2011, MNRAS, 410, 1631
Ford E. B., 2006, ApJ, 642, 505
Guillot T., Showman A. P., 2002, A&A, 385, 156
Kovács G., Zucker S., Mazeh T., 2002, A&A, 391, 369
Kovács G., Bakos G., Noyes R. W., 2005, MNRAS, 356, 557
Kurucz R. L., 1992, in Barbuy B., Renzini A., eds, Proc. IAU Symp. 149, The Stellar Populations of Galaxies. Kluwer Academic Publishers, Dordrecht, p. 225
Latham D. W. et al., 2009, ApJ, 704, 1107
Laughlin G., Crismani M., Adams F. C., 2011, ApJ, 729, L7
Lucy L. B., Sweeney M. A., 1971, AJ, 76, 544
Mandel K., Agol E., 2002, ApJ, 580, L171
Mordasini C., Alibert Y., Benz W., Naef D., 2009, A&A, 501, 1161
Morton T. D., Johnson J. A., 2011, ApJ, 729, 138
Pollacco D. L. et al., 2006, PASP, 118, 1407
Pollacco D. et al., 2008, MNRAS, 385, 1576
Queloz D. et al., 2001, A&A, 379, 279
Rowe J. F. et al., 2008, ApJ, 689, 1345
Schneider J., Dedieu C., Le Sidaner P., Savalle R., Zolotukhin I., 2011, A&A, in press
Tamuz O., Mazeh T., Zucker S., 2005, MNRAS, 356, 1466
Torres G., Neuhäuser R., Guenther E. W., 2002, AJ, 123, 1701
Yi S. K., Kim Y.-C., Demarque P., 2003, ApJS, 144, 259

This paper has been typeset from a TEX/LATEX file prepared by the author.